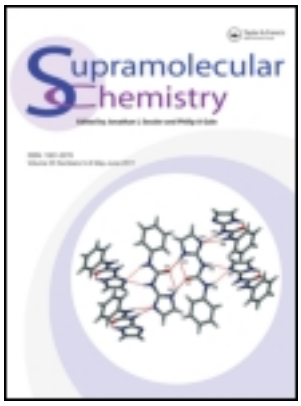

Supramolecular Chemistry
Publication details, including instructions for authors and subscription information:
http://www.tandfonline.com/loi/gsch20

Controlled assembly of heterometallic lanthanide(III) macrocycles: incorporation of photoactive and highly paramagnetic metal centres within a single complex

David J. Lewis [a], Federica Moretta [a] & Zoe Pikramenou [a]
[a] School of Chemistry, University of Birmingham, Edgbaston, Birmingham, B15 2TT, UK

Available online: 20 Mar 2012

To cite this article: David J. Lewis, Federica Moretta & Zoe Pikramenou (2012): Controlled assembly of heterometallic lanthanide(III) macrocycles: incorporation of photoactive and highly paramagnetic metal centres within a single complex, Supramolecular Chemistry, 24:2, 135-142

To link to this article: http://dx.doi.org/10.1080/10610278.2011.632823

Supramolecular Chemistry
Vol. 24, No. 2, February 2012, 135–142

Controlled assembly of heterometallic lanthanide(III) macrocycles: incorporation of photoactive and highly paramagnetic metal centres within a single complex

David J. Lewis, Federica Moretta and Zoe Pikramenou*

School of Chemistry, University of Birmingham, Edgbaston, Birmingham, B15 2TT, UK

(*Received 18 July 2011; final version received 13 October 2011*)

Building on the recent discovery that heterometallic lanthanide complexes can be assembled in a controlled manner using thiol–disulphide chemistry, we now present the assembly of macrocycles that contain both photoactive and highly paramagnetic centres as potential bimodal probes. The assembly of macrocycles **M1** and **M2** was monitored by UV–visible absorption spectroscopy and electrospray mass spectrometry. Macrocycle **M1** contains both Eu^{3+} and Gd^{3+} lanthanide centres, and has potential as a dual output probe for visible emission and magnetic resonance imaging measurements. The Eu^{3+} emission is perturbed compared to an isoabsorptive non-macrocyclic equivalent complex, **EuL^{x}**. Macrocycle **M2** incorporates Eu^{3+} and Nd^{3+} lanthanide centres for dual optical output in the visible and near-infrared regions of the electromagnetic spectrum. We demonstrate that in **M2** there is a quenching effect on the Eu^{3+} centre, caused by the presence of the proximal Nd^{3+} centre, attributed to energy transfer from Eu^{3+} to Nd^{3+}.

Keywords: lanthanide luminescence; heterometallic complexes; near-infrared emission; magnetic resonance imaging

1. Introduction

In biomedical imaging, it is challenging to find a single probe that will fulfil all requirements for detection including spatial resolution, time limitations and sensitivity. Consequently, the design of multifunctional probes which incorporate two or more imaging modalities within the same molecular architecture has recently attracted great interest (*1*). Such probes offer the opportunity to use complementary imaging modes that greatly increase the sensitivity and spatial resolution in imaging applications compared to the single outputs (*2*). Multimodal imaging probes ensure that the detected signals are co-localised within a tissue, and the problem of differing pharmacokinetic profiles for a pair of single probes is circumvented by the use of a bimodal probe incorporating the chosen outputs. Multimodal probes are a real-life case of where 'the sum is greater than the parts'.

Incorporation of two or more trivalent lanthanide (Ln) ions into organic ligand architectures presents opportunities for the design and realisation of bimodal probes. The well-known emission from Ln^{3+} ions, which arises from the Laporte-forbidden radiative *f–f* transitions from an excited luminescent state to a ground state manifold, is line-like and long-lived and thus highly suited for imaging applications in a biological forum (*3*, *4*). As the energy of the emission is dictated by the energy gap between the luminescent electronic state and the ground state manifold for each ion, the optical emission output wavelength of a luminescent Ln^{3+} complex can be easily selected by judicious choice of the lanthanide centre; essentially 'choose the lanthanide – dial a colour'. Consideration of the size of the aforementioned energy gaps and the lack of interference from phonon-mediated pathways in solution, certain lanthanides are expected to emit in the visible (Vis) region (Sm^{3+}, Eu^{3+}, Tb^{3+} and Dy^{3+}), while others emit predominantly in the near-infrared region (NIR) of the electromagnetic spectrum (Pr^{3+}, Nd^{3+}, Ho^{3+}, Er^{3+} and Yb^{3+}). The NIR-emitting lanthanides, in particular Yb^{3+} and Nd^{3+}, have potential in biological imaging applications due to the inherent transparency of biological tissues to wavelengths of light in the range of 0.8–1.2 μm. The design of ligands which can indirectly populate the lanthanide luminescent state (*5*) efficiently while protecting the ion from quenching species, such as water, by saturated coordination (*6*) or hydrophobic effects (*7*) can effectively preclude the problem associated with population of the Ln^{3+} excited states by direct excitation of the ion, which, due to the forbidden nature of the *f–f* transitions, is an inefficient process ($\varepsilon \sim 1$–$10\,mol^{-1}\,dm^3\,cm^{-1}$). The coordination chemistry of the lanthanide ions is similar across the period due to the predominance of the +3 oxidation state combined with the minimal crystal field effects imposed by the metal centre. Hence, the coordination preferences of the emissive lanthanide ions are almost identical to the Gd^{3+} ion that is well known for providing T1 contrast in magnetic resonance imaging (MRI) (*8*). Heterometallic lanthanide complexes are therefore an attractive target as potential

*Corresponding author. Email: z.pikramenou@bham.ac.uk

ISSN 1061-0278 print/ISSN 1029-0478 online

http://dx.doi.org/10.1080/10610278.2011.632823
http://www.tandfonline.com

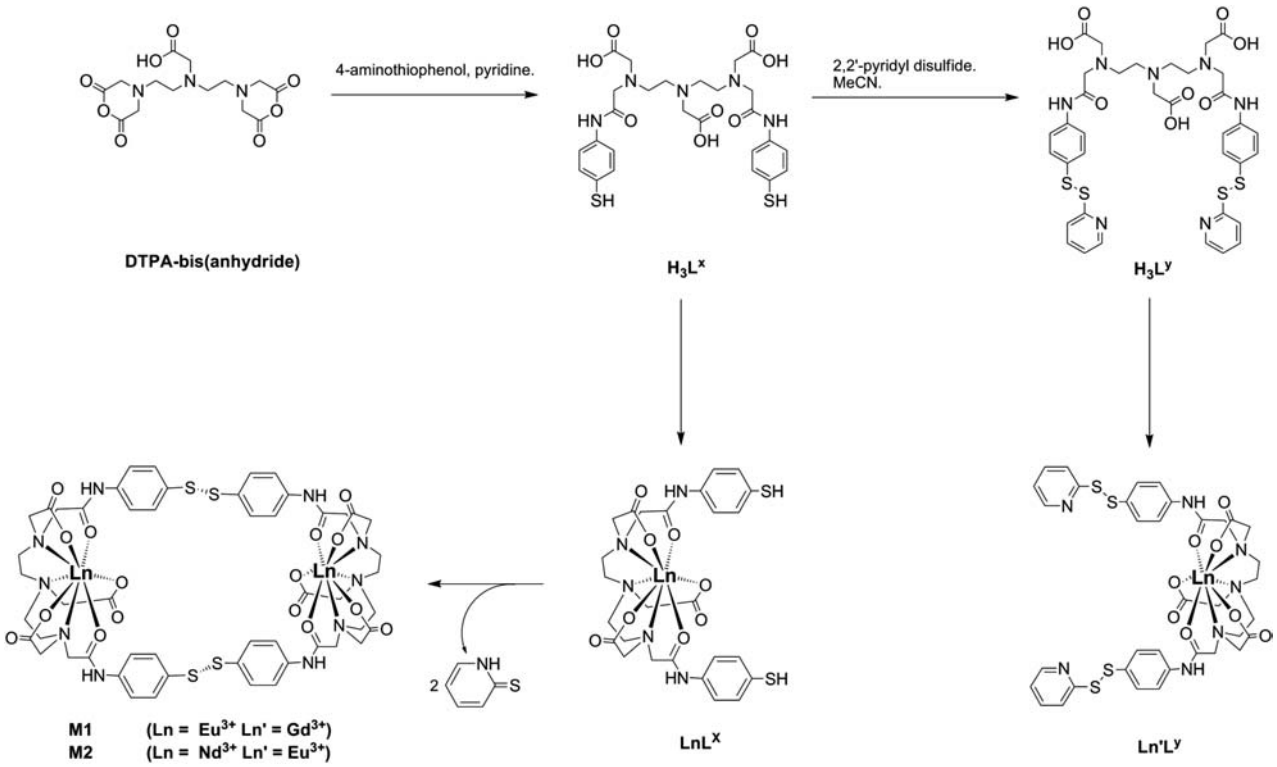

Scheme 1. Synthetic route to macrocycles **M1** and **M2** by controlled assembly of disulphide bonds.

multimodal probes that can incorporate the desired luminescent properties (Vis/NIR) with magnetic properties (MRI) using a combination of metal centres. However, due to the similar coordination preferences of the lanthanide(III) ions, it is a challenge to synthesise heterometallic lanthanide complexes. Previous approaches have included assembly by discrimination of ionic radius or 'statistical crystallisation' (*9–17*). We recently reported the synthesis and characterisation of a purely heterometallic EuTb macrocyclic species by the controlled assembly of disulphide bonds (*18*). The reaction between 2-pyridyl disulphide groups with thiols is well known as a mild and selective method for the assembly of disulphide bonds (*19*). Mechanistically, the reaction proceeds as a thiol–disulphide exchange which has been exploited to a great effect by Otto and Sanders in the production of 'dynamic combinatorial libraries' which, through the reversible nature of the exchange process, allow the production of the most efficient macrocyclic host for a targeted guest molecule (*20*, *21*); in many cases the process ends in a global energy minimum for each host–guest system. However, unlike the thiol–disulphide exchange reaction used in the aforementioned body of work, the thiol–disulphide exchange between $\mathbf{LnL^x}$ and $\mathbf{Ln'L^y}$ to produce either **M1** or **M2** (Scheme 1) is not reversible, due to the predominance of the 2-pyridyl thione tautomer of 2-thiopyridine at room temperature (*22*), and is consequently under kinetic control. Macrocyclic species can, therefore, be trapped out and analysed.

2. Results and discussion

2.1 Controlled assembly of EuGd (M1) and NdEu (M2) macrocycles

$\mathbf{H_3L^x}$ was synthesised using the dual acylation procedure described by Lewis et al. (Scheme 1) (*18*). Characterisation of the product by ^{1}H NMR spectroscopy was entirely consistent with the results previously observed. Positive-mode electrospray mass time-of-flight spectrometry (ES-TOF-MS) was used to confirm the correct molecular weight of $\mathbf{H_3L^x}$. The UV–Vis absorption spectrum of $\mathbf{H_3L^x}$ confirmed the presence of the $\pi-\pi^*$ electronic transition of the thiophenyl chromophores as a broad, high-energy transition ($\lambda_{max} = 266$ nm).

The synthesis of $\mathbf{H_3L^y}$, using the previously described synthetic procedure that is based on thiol–disulphide exchange between $\mathbf{H_3L^x}$ and an excess of 2,2′-pyridyl disulphide to generate the product, also proceeded as expected. The characterisation of the reaction product by ^{1}H NMR and ES-TOF-MS demonstrated that the synthesis had been successful. The appearance of the shoulder at 285 nm in the UV–Vis absorption spectrum of $\mathbf{H_3L^y}$ corresponding to the $\pi-\pi^*$ electronic transition of the

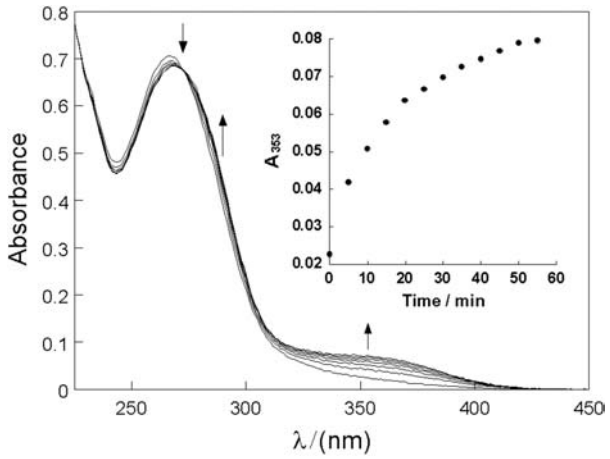

Figure 1. UV–Vis absorption spectra of a solution containing **EuL^x** (25 μM) and **GdL^y** (25 μM) in methanol at time intervals of 0, 5, 10, 15, 20, 25 and 30 min after mixing of solutions. Inset: monitoring formation of **M1** by absorbance at 353 nm for the same experiment.

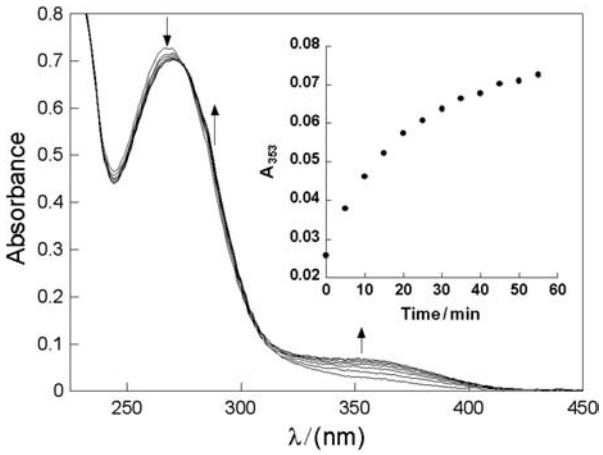

Figure 2. UV–Vis absorption spectra of a solution containing **NdL^x** (25 μM) and **EuL^y** (25 μM) in methanol at time intervals of 0, 5, 10, 15, 20, 25 and 30 min after mixing of solutions. Inset: monitoring formation of **M2** by absorbance at 353 nm for the same experiment.

pyridyl group demonstrated that the heterocyclic moiety is incorporated into the ligand framework.

Macrocycle **M1** was assembled from a mixture of **EuL^x** and **GdL^y**. The lanthanide complexes were made *independently* by the mixing of the corresponding ligand with the lanthanide salt. The progress of reaction was monitored by the release of 2-pyridyl thione, itself a chromophore with an absorption maxima at 353 nm, using UV–Vis absorption spectroscopy. Sequential overlaid spectra taken every 5 min for 1 h showed that the absorption of the shoulder at 285 nm, corresponding to the pyridyl group incorporated in **GdL^y** is reduced over time, while the peak corresponding to the release of 2-pyridyl thione, the signature for reaction and production of **M1**, is enhanced (Figure 1). A plot of absorbance at 355 nm vs. time demonstrates two-step reaction kinetics, with a rapid first step involving the reaction of one pendant arm of **EuL^x** and **GdL^y**, respectively, followed by a slow reorganisation-ring closing step by which the macrocyclic species **M1** is formed. This behaviour is entirely consistent with that observed for the formation of the EuTb macrocycle described previously by us (*18*).

Likewise, macrocycle **M2** was assembled from a mixture of **NdL^x** and **EuL^y**. The reaction was monitored by UV–Vis absorption spectroscopy, and gave an identical result to that for the formation of **M1**, with the same two-step association–cyclisation phenomena observed by monitoring the absorption at 353 nm of released 2-pyridyl thione (Figure 2). Control experiments performed using mixtures of **LnL^x** and **Ln′L^x** formed *in situ*, at the same concentrations used to assemble the macrocyclic species, demonstrated that there were no changes in the UV–Vis absorption spectrum over the same time period when the pyridyl disulphide activated lanthanide complexes **Ln′L^y** were not present in the reaction mixture.

Positive-mode electrospray mass spectrometry was used to confirm the molecular weight of macrocycle **M1** (Figure 3). A peak at *m*/*z* 778 was observed in the mass spectrum of **M1** corresponding to the doubly charged $[\mathbf{M1} + K + H]^{2+}$ ion, which is consistent with the ionisation mode of these macrocyclic species (*18*). Likewise, a peak at *m*/*z* 774 was observed in the mass spectrum of **M2**, corresponding to the doubly charged $[\mathbf{M2} + Na + Na]^{2+}$ ion. In the case of both **M1** and **M2**, the isotope patterns observed served as the signature of dual lanthanide incorporation. Peaks corresponding to species generated by either **LnL^x** or **Ln′L^y** were not observed in either spectrum, demonstrating that **M1** and **M2** are the major species generated in thiol–disulphide exchange reaction to produce heterometallic macrocycles. Likewise, no peaks corresponding to homometallic species, which could have been attributed to statistical assembly, were observed.

2.2 Photophysical studies of heterometallic macrocycles

Both macrocyclic species **M1** and **M2** contain photoactive lanthanide metallocentres. **M1** incorporated an Eu^{3+} centre in the same molecular edifice as a Gd^{3+} centre, whereas **M2** possessed two photoactive lanthanide centres, Eu^{3+}, which emits in the visible, and Nd^{3+}, which emits in the NIR region of the electromagnetic spectrum.

Initially, we studied the photophysical properties of the Eu^{3+} centre in **M1** under steady-state conditions. Typical Eu^{3+} luminescence was observed in the region 570–720 nm after excitation into the phenyl chromophore

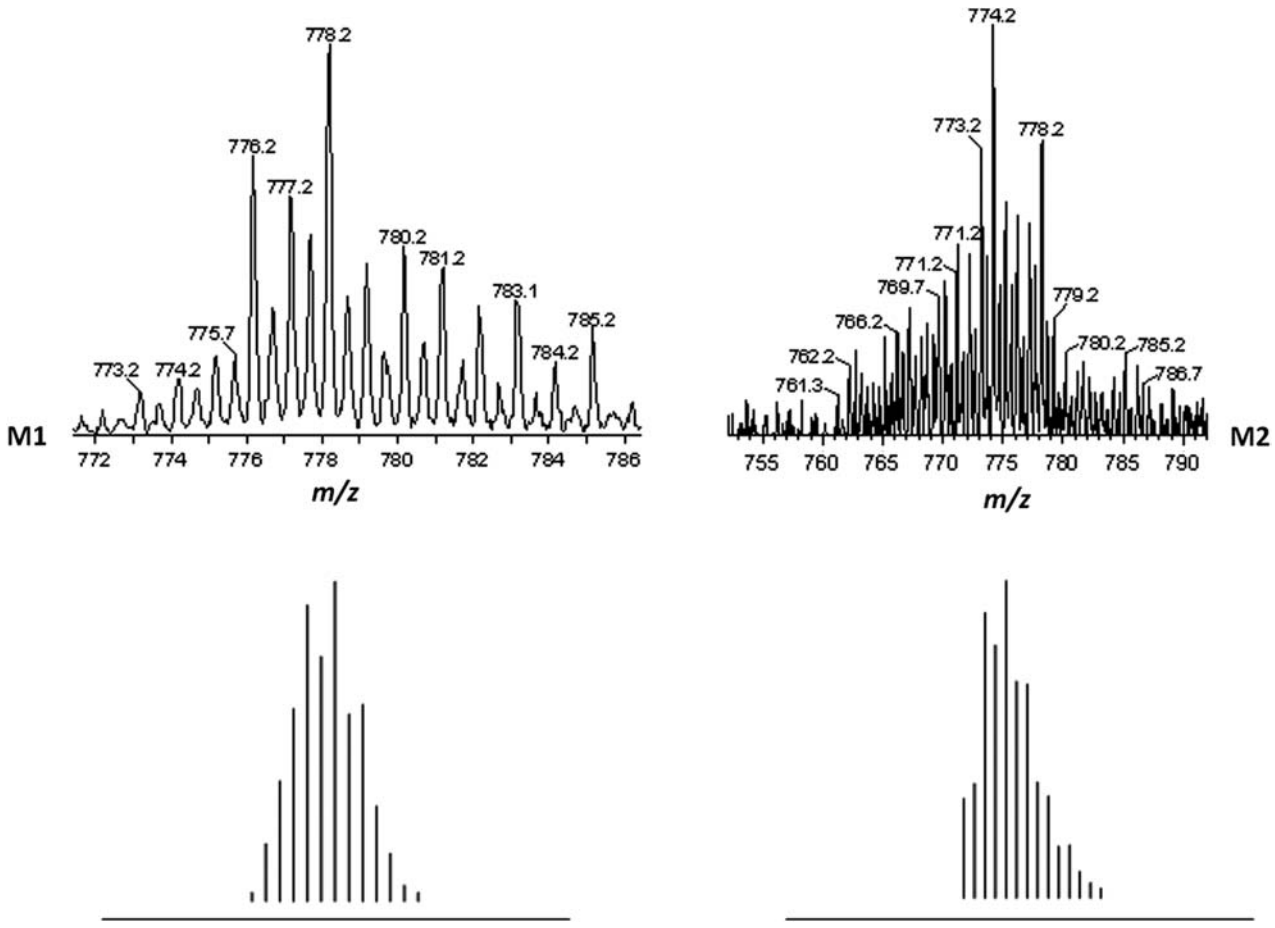

Figure 3. ES-TOF^{+}-MS of macrocyclic lanthanide species **M1** (EuGd) and **M2** (EuNd). Bottom: theoretical isotope patterns. Top: observed isotope patterns and associated peak *m*/*z*.

absorption band at 266 nm (Figure 4). The narrow emission bands at 580, 590, 614, 650 and 694 nm correspond to the $^{5}D_0 \rightarrow {}^{7}F_J$ *f*–*f* transitions in Eu^{3+} where

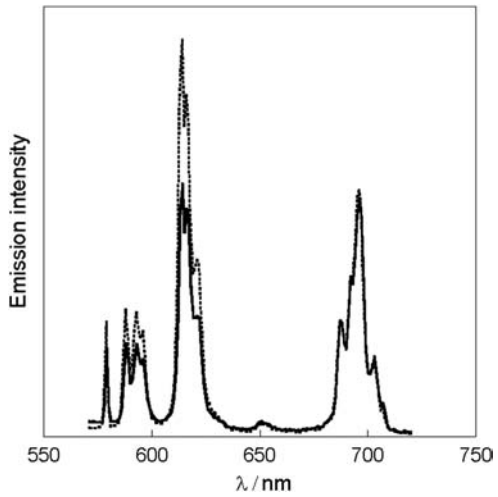

Figure 4. Overlay of corrected emission spectra of **M1** (—) and an isoabsorptive mixture of 1:1 $\mathbf{EuL^x}$–$\mathbf{GdL^x}$ (···) in methanol-*d*. $\lambda_{exc} = 266$ nm.

$J = 0$, 1, 2, 3 and 4, respectively. An excitation spectrum recorded in the range of 200–450 nm by monitoring the emission of the most intense Eu^{3+} emission band at 614 nm ($^{5}D_0 \rightarrow {}^{7}F_2$) gave a maximum at around 265 nm, demonstrating that energy transfer from the phenyl chromophore to the lanthanide centre is responsible for the sensitised lanthanide emission observed (Supplementary Information available online). As a result, the complexes possess a large Stokes shift ($\lambda_{em}-\lambda_{exc}$) of over 300 nm; typically organic chromophores have Stokes shifts <50 nm, thus scattering of excitation light is a problem circumvented by the use of lanthanide(III) complexes as probes. The indirect population of the lanthanide luminescent state (sensitisation of emission) by organic chelating ligands is widely accepted to proceed predominantly through the excited ligand triplet state (T_1) after an intersystem crossing from the singlet ligand excited state (S_1). This energy transfer pathway was first alluded to by Crosby in the study of rare earth chelates with 8-hydroxyquinolinates (*23*) and later observed directly by Nocera (*24*). To examine the effect of the proximity of the Gd centre as a heavy atom on the

luminescence properties of Eu^{3+}, isoabsorptive solutions of **M1** and a 1:1 mixture of $\mathbf{EuL^x}$ and $\mathbf{GdL^x}$ were studied by steady-state luminescence spectroscopy. The emission was studied in methanol-*d* to preclude quenching pathways caused by OH oscillators, and for comparative purposes to the NIR-emitting **M2** (vide infra). In both cases, narrow-band Eu^{3+} emission in the range of 570–720 nm was observed after the excitation of the ligand absorption band at 266 nm. It was found that the Eu^{3+} emission of **M1** was decreased by 15% compared to the non-macrocyclic $\mathbf{EuL^x}$–$\mathbf{GdL^x}$ cocktail (Figure 4). However, only the *f*–*f* transitions for $J = 1$ and 2 of Eu^{3+} at 590 and 614 nm, respectively, in **M1** were reduced in intensity compared to the emission observed for the $\mathbf{EuL^x}$–$\mathbf{GdL^x}$ mixture; the $J = 0$, 3 and 4 *f*–*f* transitions were relatively unperturbed. The lifetime of the europium centre in **M1** monitored at 614 nm ($^5D_0 \rightarrow {}^7F_2$) was found to be 1.53 ms, compared to 1.61 ms in the non-macrocyclic isoabsorptive 1:1 $\mathbf{EuL^x}$–$\mathbf{GdL^x}$ mixture. This observation mirrors the 15% reduction in emission intensity observed in the steady-state spectra, and although the effect is small it is clearly demonstrated in the macrocycle case, and can be attributed to different factors. Photo-induced energy transfer from Eu^{3+} to Gd^{3+} is excluded as a possible pathway of quenching of the europium emission, since energy cannot be passed from the luminescent level in europium to the Gd^{3+} centre, which is energetically mismatched ($^6P_{7/2}$ state at 32,000 cm^{-1}). Another possibility is the effect of the Gd as an internal heavy atom. This effect is a well-known phenomenon that usually increases the rate of intersystem crossing of an organic fluorophore from S_1 to T_1; the spin inversion in the organic chromophore is assisted by spin–orbit coupling to the heavy atom and is proportional to atomic number (*Z*) (*25*). The presence of the proximal Gd^{3+} centre within **M1** could therefore either increase the rate of intersystem crossing in the phenyl chromophore, or could increase the rate of non-radiative pathways of emission, which is more likely to be occurring in this case. This is supported by the changes in the steady-state emission spectrum, where the magnetic dipole $^5D_0 \rightarrow {}^7F_1$ and the hypersensitive $^5D_0 \rightarrow {}^7F_2$ *f*–*f* transitions are mostly affected.

Heterometallic macrocycle **M2**, which was designed to contain dual emission output in the visible (Eu^{3+}) and NIR (Nd^{3+}) regions of the electromagnetic spectrum, was studied by steady-state emission techniques. Two separate sets of narrow emission bands were observed in the ranges of 570–720 and 850–1350 nm after excitation in the ligand absorption maxima at 266 nm in methanol-*d*. Emission of Eu^{3+} gives rise to the bands at 580, 590, 614, 650 and 694 nm corresponding to the $^5D_0 \rightarrow {}^7F_J$ *f*–*f* transitions in Eu^{3+} where $J = 0$, 1, 2, 3 and 4, respectively (Figure 5). Likewise, the emission of Nd^{3+} within the same molecule gives rise to the bands observed at 890, 1064 and 1350 nm, corresponding to the $^4F_{3/2} \rightarrow {}^4I\text{-}_J$ *f*–*f* transitions in Nd^{3+} where $J = 9/2$, 11/2 and 13/2, respectively (Figure 6).

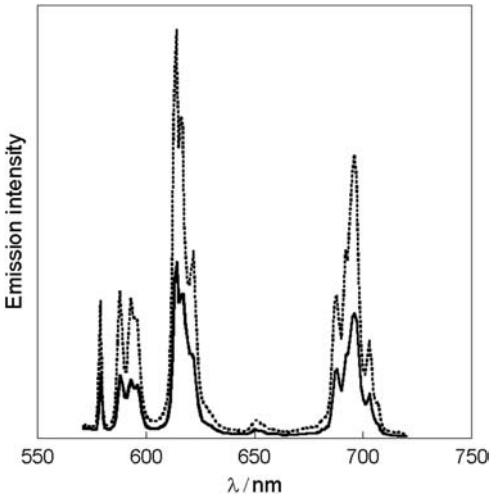

Figure 5. Overlay of corrected emission spectra of **M2** (—) and an isoabsorptive mixture of 1:1 $\mathbf{EuL^x}$–$\mathbf{NdL^x}$ (···) in methanol-*d*. $\lambda_{exc} = 266$ nm.

Excitation spectra monitored at the most intense emission band for each lanthanide centre (Eu^{3+}, 614 nm; Nd^{3+}, 1064 nm) demonstrated that an energy transfer from the phenyl chromophore in **M2** is responsible for the sensitised emission observed for both Nd^{3+} and Eu^{3+} centres within the same complex (Supplementary Information available online). Comparison of the emission of isoabsorptive solutions of 1:1 $\mathbf{EuL^x}$–$\mathbf{NdL^x}$ with **M2** demonstrated that the Eu^{3+} emission in **M2** is quenched (Figure 5). A study of the lifetime of Eu^{3+} monitored at 614 nm ($^5D_0 \rightarrow {}^7F_2$) in both **M2** showed that the lifetime

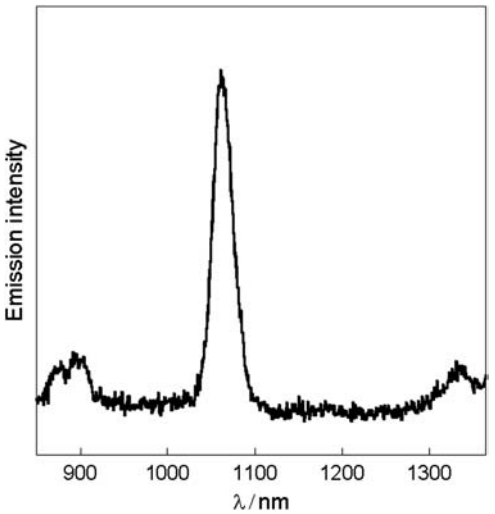

Figure 6. Emission spectrum of **M2** in methanol-*d* focused on the NIR region. $\lambda_{exc} = 266$ nm.

had been reduced to 0.69 ms. We propose that an energy transfer occurs from Eu^{3+} (donor) to Nd^{3+} (acceptor), which causes both a characteristic reduction in steady-state emission intensity and luminescent-state lifetime of Eu^{3+} in macrocyclic **M2** compared to the 1:1 **EuL^{x}–NdL^{x}** mixture. Energy transfer is expected to proceed from the $^5D_0$ state of Eu^{3+} into either the ^4G_J or ^4F_J manifolds of Nd^{3+}, predominantly by a dipole–dipole through-space energy transfer process (*26*). However, when we compared the steady-state emission of Nd^{3+} in **M2** and1:1 **EuL^{x}–NdL^{x}** mixture, there is no apparent increase in the emission of the donor, Nd^{3+} as might be expected for a standard donor–acceptor pair either by steady-state or time-resolved luminescence spectroscopies. This effect, however, has been noted previously for Eu^{3+} and Nd^{3+} ions held in close proximity within silicate glasses (*27*); energy transfer observed from Eu^{3+} to Nd^{3+}, which led to a reduction of the Eu^{3+} luminescence did not necessarily increase the Nd^{3+} luminescence. Energy transfer from Tb^{3+} to Yb^{3+} has been observed previously in a diethylenetriamine penta-acetic acid (DTPA) bisamide trinuclear complex (*28*). Assuming that the energy transfer proceeds from a single donor to a single acceptor, the energy transfer efficiency (η) between lanthanide centres within **M2** can be calculated using the following relationship:

$$\eta = 1 - (\tau/\tau_0), \tag{1}$$

where τ is the observed lifetime of the donor in the presence of the acceptor species and τ_0 the lifetime of the donor in the absence of the acceptor. Using the reported lifetime of **EuL^{x}** in methanol-*d* ($\tau_0 = 1.75$ ms) (*18*) and the lifetime of the Eu^{3+} centre in **M2** in methanol-*d* ($\tau = 0.69$ ms) monitored at the $^5D_0 \rightarrow {}^7F_2$ *f–f* transition at 614 nm after excitation at 266 nm, the efficiency of the energy transfer from Eu^{3+} to Nd^{3+} was found to be 61%. Using this value, and the relationship

$$\eta = \frac{1}{\left[1 + (R/R_0)^6\right]}, \tag{2}$$

where R_0 is the distance between Eu^{3+} and Nd^{3+} required for 50% energy transfer efficiency (reported to be 9.2 Å by Horrocks Jr. and Sudnick (*29*)), the actual distance between Eu^{3+} and Nd^{3+} within the molecular architecture, *R*, was calculated as 8.5 Å, which is consistent with the previously reported MM2 model of the analogous EuTb macrocycle, which shares a common ligand architecture with **M2**, and a reported inter-lanthanide distance in the pseudo-*endo* state of 7.8 Å. We therefore conclude that the energy transfer mechanism when Eu^{3+} is a donor and an NIR lanthanide is an acceptor follows the same kinetic behaviour as in the case of the two visible-emitting lanthanides.

3. Conclusion

We have shown the assembly of heterometallic macrocycles **M1**, incorporating both Eu^{3+} and Gd^{3+} centres, and **M2** incorporating Eu^{3+} and Nd^{3+} centres, using the controlled assembly of disulphide bonds. **M1** presented emission from the Eu^{3+} centre, sensitised through the ligand framework, which was perturbed by the presence of Gd^{3+}. **M2**, which incorporated both Eu^{3+} and Nd^{3+} presents dual output luminescence in the visible and the NIR regions of the electromagnetic spectrum after excitation into a common ligand sensitiser. It was possible to elucidate an energy transfer from Eu^{3+} to Nd^{3+} was active in **M2**, with the efficiency of the inter-lanthanide intramolecular energy transfer process was calculated to be 61%, which is consistent with the previous findings that the energy transfer step proceeds through the pseudo-*endo* state of the macrocycle, where the lanthanide ions are separated by a distance of around 8 Å. These results show the importance of the proximity of the lanthanide centres for the design of multimodal probes based on lanthanides.

4. Experimental

4.1 Materials and instrumentation

All chemicals were purchased from Acros and Sigma-Aldrich. Solvents were purchased from Sigma-Aldrich or Fisher. Deuterated solvents were purchased from Goss Scientific or Aldrich and used as received. Diethylenetriamine-*N*,*N*′,*N*″-triacetic-*N*,*N*″-dianhydride [DTPA-bis(anhydride)] was synthesised as reported previously (*18*). HPLC grade solvents were used in photophysical studies. Water was deionised using an Elga Option 3 water purifier. Pyridine was dried over activated 4 Å molecular sieves. All ligand and complex synthetic procedures were carried out under dinitrogen with degassed anhydrous solvents. ^{1}H NMR spectra were obtained using a Bruker AVIII300 spectrometer and ^{13}C {^{1}H} polarisation enhancement nurtured during attached nucleus testing (PENDANT) NMR spectra were obtained using a Bruker AVIII400 spectrometer. Electrospray mass spectra were recorded on Micromass LC-TOF machine.

Steady-state luminescence experiments were carried out using either the Photon Technology International fluorescence system previously described (*18*), or using an Edinburgh instruments FLS920 system equipped with a 450 W Xenon lamp and double excitation and emission monochromators. Detection of emitted photons was achieved by the use of an air-cooled Hamamatsu R928 (Vis – red sensitive) photomultiplier tube or a liquid nitrogen-cooled Hamamatsu 5582-17 (NIR sensitive) photomultiplier tube.

Emission lifetimes were recorded using the third harmonic (355 nm) of a Continuum Surelite I SSP class 4

pulsed Nd-YAG laser (10 Hz), or using an Edinburgh Instruments μF microsecond flash lamp (1–1000 Hz) as excitation source. Lifetime data were recorded using the multi-channel scaling single-photon counting method. Detector saturation was avoided in all circumstances by using minimal signal rate intensities combined with extended data collection times. Lifetime data were fitted to exponential decays using the tail fit option in Edinburgh Instruments F900 PC software. UV–Vis absorption spectra were recorded using either a Varian Cary 50 single beam spectrometer or a Varian Cary 5000 dual beam spectrometer.

4.2 N,N″-*bis*(p-*thiophenolamide)diethylenetriamine*-N,N′,N″-*triacetic acid,* H_3L^x

The synthetic route of this compound has been fully described previously by Pikramenou and co-workers (*18*). All characterisation data were consistent with that previously reported: ^{1}H NMR (300 MHz, d_4-MeOH), δ ppm: 7.40 (4H, d); 7.13 (4H, d); 4.12 (2H, s); 3.62 (4H, s); 3.59 (4H, s); 3.49 (4H, t); 3.22 (4H, t). MS (ES-TOF$^+$): *m/z* 608 $[M + H]^+$, 630 $[M + Na]^+$. UV–Vis (MeOH): λ_{max} in nm (log ε) 264 (4.4).

4.3 N,N″-*bis*(p-*pyridyldisulphidephenylamide)diethylenetriamine*-N,N′,N″-*triacetic acid,* H_3L^y

The synthesis of this compound has been fully described previously by Pikramenou and co-workers (*18*).

All characterisation data were consistent with that previously reported: ^{1}H NMR (300 MHz, d_4-MeOH), δ ppm: 8.45 (2H, m), 7.77 (4H, m), 7.44 (4H, d), 7.31 (4H, d), 7.22 (2H, m), 4.39 (2H, s), 3.70 (4H, s), 3.63 (4H, s), 3.53 (4H, t), 3.22 (4H, t). MS (ES-TOF$^+$) *m/z*: 826 $[M + H]^+$, 848 $[M + Na]^+$. UV–Vis (MeOH) λ_{max} in nm (log ε): 262 (4.5), 285(sh) (4.4).

4.3.1 Formation of dinuclear heterometallic macrocycles: M1 and M2

Stock solutions (1 mM) of $\mathbf{H_3L^x}$, $\mathbf{H_3L^y}$, $LnCl_3.6H_2O$ and $Ln'Cl_3.6H_2O$ in methanol or methanol-*d* were initially prepared (**M1**: Ln = Eu^{3+}, Ln′ = Gd^{3+}; **M2**: Ln = Nd^{3+}, Ln′ = Eu^{3+}). The stock solutions were then used to form $\mathbf{LnL^x}$ and $\mathbf{Ln'L^y}$ species directly in solution (1:1 molar ratio of ligand to lanthanide) at a concentration of 25 μmol dm^{-3} by simple mixing and dilution in methanol or methanol-*d*. Equal volumes of the solutions of $\mathbf{LnL^x}$ and $\mathbf{Ln'L^y}$ were then combined rapidly with vigorous stirring and macrocycle formation was monitored by UV–Vis absorption spectroscopy over 1 h. The concentration of the macrocyclic species after mixing is 12.5 μmol dm^{-3}. Macrocycles were characterised by positive-mode electrospray mass spectrometry and steady-state and time-resolved luminescence spectroscopy.

Acknowledgements

We wish to thank the European Community Action Scheme for the Mobility of University Students (ERASMUS), and COST action D38 'Metal-Based Systems for Molecular Imaging Applications' and EPSRC for funding. Some of the spectrometers used in this research were obtained, through Birmingham Science City: Innovative Uses for Advanced Materials in the Modern World (West Midlands Centre for Advanced Materials Project 2), with support from Advantage West Midlands (AWM) and part funded by the European Regional Development Fund (ERDF).

References

(1) Louie, A. *Chem. Rev.* **2010**, *110*, 3146–3196.
(2) Hahn, M.; Singh, A.K.; Sharma, P.; Brown, S.C.; Moudgil, B.M. *Anal. Bioanal. Chem.* **2011**, *399*, 3–27.
(3) Bunzli, J.-C.G. *Chem. Rev.* **2010**, *110*, 2729–2755.
(4) Montgomery, C.P.; Murray, B.S.; New, E.J.; Pal, R.; Parker, D. *Acc. Chem. Res.* **2009**, *42*, 925–937.
(5) Moore, E.G.; Samuel, A.P.S.; Raymond, K.N. *Acc. Chem. Res.* **2009**, *42*, 542–552.
(6) Nonat, A.; Imbert, D.; Pecaut, J.; Giraud, M.; Mazzanti, M. *Inorg. Chem.* **2009**, *48*, 4207–4218.
(7) Magennis, S.W.; Parsons, S.; Pikramenou, Z. *Chem. Eur. J.* **2002**, *8*, 5761–5771.
(8) Caravan, P.; Ellison, J.J.; McMurry, T.J.; Lauffer, R.B. *Chem. Rev.* **1999**, *99*, 2293–2352.
(9) Andre, N.; Jensen, T.B.; Scopelliti, R.; Imbert, D.; Elhabiri, M.; Hopfgartner, G.; Piguet, C.; Bünzli, J.-C.G. *Inorg. Chem.* **2004**, *43*, 515–529.
(10) Andre, N.; Scopelliti, R.; Hopfgartner, G.; Piguet, C.; Bünzli, J.-C.G. *Chem. Commun.* **2002**, 214–215.
(11) Canard, G.; Koeller, S.; Bernardinelli, G.; Piguet, C. *J. Am. Chem. Soc.* **2008**, *130*, 1025–1040.
(12) Costes, J.-P.; Dahan, F.; Dupuis, A.; Lagrave, S.; Laurent, J.-P. *Inorg. Chem.* **1998**, *37*, 153–155.
(13) Costes, J.-P.; Nicodeme, F. *Chem. Eur. J.* **2002**, *8*, 3442–3447.
(14) Elhabiri, M.; Scopelliti, R.; Bünzli, J.-C.G.; Piguet, C. *J. Am. Chem. Soc.* **1999**, *121*, 10747–10762.
(15) Placidi, M.P.; Villazara, A.J.L.; Natrajan, L.S.; Sykes, D.; Kenwright, A.M.; Faulkner, S. *J. Am. Chem. Soc.* **2009**, *131*, 9916–9917.
(16) Tremblay, M.S.; Sames, D. *Chem. Commun.* **2006**, 4116–4118.
(17) Natrajan, L.S.; Villaraza, A.J.L.; Kenwright, A.M.; Faulkner, S. *Chem. Commun.* **2009**, 6020–6022.
(18) Lewis, D.J.; Glover, P.B.; Solomons, M.C.; Pikramenou, Z. *J. Am. Chem. Soc.* **2011**, *133*, 1033–1043.
(19) Hermanson, G.T. *Bioconjugate Techniques*; Academic Press: San Diego, CA, 1996.
(20) Otto, S.; Furlan, R.L.E.; Sanders, J.K.M. *Science* **2002**, *297*, 590–593.
(21) Au-Yeung, H.Y.; Pengo, P.; Panto, G.D.; Otto, S.; Sanders, J.K.M. *Chem. Commun.* **2009**, 419–421.

(22) Alam, M.M.; Fujitsuka, M.; Watanabe, A.; Ito, O. *J. Chem. Soc. Perkin Trans.* **1998**, *2*, 817–824.
(23) Crosby, G.A.; Whan, R.E.; Alire, R.M. *J. Chem. Phys.* **1961**, *34*, 743–748.
(24) Yu, J.; Lessard, R.B.; Bowman, L.E.; Nocera, D.G. *Chem. Phys. Lett.* **1991**, *187*, 263–268.
(25) Pownall, H.J.; Granoth, I. *J. Phys. Chem.* **1976**, *80*, 508–511.
(26) Joshi, J.C.; Pandey, N.C.; Joshi, B.C.; Belwal, R.; Joshi, J. *J. Solid State Chem.* **1978**, *23*, 135–139.
(27) Sharp, E.J.; Weber, M.J.; Cleek, G. *J. App. Phys.* **1970**, *41*, 364–369.
(28) Faulkner, S.; Pope, S.J.A. *J. Am. Chem. Soc.* **2003**, *125*, 10526–10527.
(29) Horrocks, Jr, W.W.; Rhee, M.-J.; Snyder, A.P.; Sudnick, D.R. *J. Am. Chem. Soc.* **1980**, *102*, 3650–3652.